Copper, gold, and platinum under femtosecond irradiation: Results of first-principles calculations

N. A. Smirnov*

FSUE RFNC-VNIITF named after academ. E. I. Zababakhin, 456770, Snezhinsk, Russia

(Received 19 December 2019; accepted 24 February 2020; published 16 March 2020)

The paper investigates the interaction of femtosecond laser pulses with the thin films of copper, gold, and platinum. It considers electron-phonon relaxation processes and melting in the metal system nonequilibrium heated by laser radiation. Instead of the approximated formula by Wang *et al.* [Phys. Rev. B **50**, 8016 (1994)], which is widely used to determine the temperature dependence of the electron-phonon coupling factor, we propose an improved approach for its more accurate calculation from first principles. Comparison with experiments and other calculations shows our approach to provide good calculation accuracy. Melting time versus absorbed energy density was estimated for the films and shown to be markedly sensitive to latent heat at low absorbed energy densities (<1 MJ/kg). Our calculations taken to study the temporal evolution of the (220) diffraction peak intensity after femtosecond irradiation show good agreement between experimental and theoretical data, which was attained due to higher accuracy in our determination of the temperature dependence electron-phonon coupling factor.

DOI: 10.1103/PhysRevB.101.094103

I. INTRODUCTION

The intensive development of femtosecond electron and x-ray diffractometry makes it possible to investigate on the atomic level the structural changes in materials irradiated by ultrashort ($\tau_p \sim 100$ fs) laser pulses [1–7]. Often studied are free-standing thin (a few tens nm) films of different materials. After arriving at the target, femtosecond irradiation (usually with optical wavelengths) heats the electronic subsystem within the penetration depth. Due to ballistic electrons which penetrate into matter to a few tens of nanometers, the electronic subsystem equilibrates during a time comparable with the pulse duration τ_p [8,9]. Here the temperature of electrons may reach a few electron volts, while ions remain relatively cold ($T \sim$ room temperature). Later their temperatures equalize gradually through electron-phonon (or electron-ion) energy relaxation processes. If the absorbed energy is above the threshold required for melting, the electron-phonon relaxation leads to lattice disordering, partial or complete [2,4,7].

As shown in experiments, material melting occurs either in the usual regime (thermal melting) during a few picoseconds (ps), and even tens and hundreds ps [2,4,7], or in the ultrafast sub-picosecond regime (nonthermal melting) during a few hundred femtoseconds [1,3,5]. In the latter case, the energy transferred to the lattice by electrons is not sufficient for melting in the ordinary way. The lattice disordering happens because of the fast change in the potential energy surface with the increasing electron temperature. As a result, the lattice loses its dynamical stability and melts [10].

Some authors [4,10–12] claim that the lattice of several metals may harden after irradiation by ultrashort laser pulses thus increasing their melting temperature. Here the change of electron-ion interaction makes the lattice more dynamically stable. But the direct observation of this effect in experiments is still questionable because of a rather high energy threshold for its detection [13] and insufficient measurement accuracy. So, for example, different experiments with the free-standing thin films of gold [4,7,13] give rather different melting times for targets irradiated by femtosecond laser pulses. Especially pronounced is the difference in experiments [7,13]. For many of the same experimental conditions (absorbed energy density ~0.36 MJ/kg), the gold target in Ref. [13] completely melts within less than 10 ps, while in Ref. [7] this time is several times longer. It seems that this disagreement is caused by substantial difference in the quality of targets used in the experiments.

The evolution of the system heated under nonequilibrium conditions by ultrashort laser pulses is usually described within the two-temperature model [14]. In order to predict structural changes on the atomic level, the two-temperature model is coupled with molecular dynamics (MD) and in this case the MD equation of atomic motion is extended by a term which accounts for energy transfer from electrons to ions [13,15–17]. The rate of energy transfer depends on the electron-phonon coupling factor [14], which is a function of electron temperature T_e [18–20]. The quality of computer simulations is to a great extent dependent on accuracy with which the temperature dependence of this factor is calculated. Although the approximate approach for predicting how the electron-phonon coupling factor varies with the increasing T_e exists [18,19], its accuracy remains questionable [7].

Having considered the drawbacks in the determination [18,19] of the electron-phonon coupling factor $G(T_e)$ as a function of electron temperature, we propose an improved approach to its calculation from first principles. The approach has helped us more accurately reproduce available experimental data. These are, first of all, the data on the temporal evolution of gold diffraction peak intensities and on $G(T_e)$

*nasmirnov@vniitf.ru

measurements after target irradiation by ultrashort laser pulses of copper [4,7,21]. The modified formula for the factor $G(T_e)$ can easily be implemented and incorporated in the existing *ab initio* codes where the electron-phonon matrix elements are calculated. In the next section we present our approach and briefly describe the *ab initio* method with its internal parameters chosen for our calculations. Section III discusses our calculated results and compares them with available experimental data for copper and gold. Also, it presents calculated results for platinum with predictions for the melting times of its thin films with respect to absorbed energy density. The last section summarizes the results we obtained.

II. CALCULATION METHOD

A. The electron-phonon coupling factor

The most widely used expression for the temperature dependence electron-phonon coupling factor $G(T_e)$ was proposed in papers [18,19] where it is written as

$$G(T_e) = \frac{2\pi\hbar k_B}{N(E_F)} \int_0^\infty \Omega\alpha^2F(\Omega)d\Omega \int_{-\infty}^\infty N^2(\varepsilon)\left(-\frac{\partial f_e}{\partial\varepsilon}\right)d\varepsilon = \frac{\pi\hbar k_B\lambda\langle\omega^2\rangle}{N(E_F)} \int_{-\infty}^\infty N^2(\varepsilon)\left(-\frac{\partial f_e}{\partial\varepsilon}\right)d\varepsilon. \quad (1)$$

Here $N(\varepsilon)$ is the density of states (DOS) for electrons with energy ε, f_e is the Fermi-Dirac distribution function of electrons, E_F is the Fermi energy, $\alpha^2F(\Omega)$ is the electron-phonon spectral distribution function calculated at $T = 0$, λ is the electron-phonon mass enhancement parameter, and $\langle\omega^2\rangle$ is the second moment of the phonon spectrum [22]. The expression was obtained within Allen formalism [23] as a generalization for high electron temperatures. The entire dependence on T_e in Eq. (1) is present in the Fermi-Dirac function derivative $(\partial f_e/\partial\varepsilon)$. Equation (1) was derived under a number of assumptions. The most important of them is approximation to the electron-phonon spectral distribution function α^2F. This function is related to the electron-phonon scattering matrix which determines the probability of electron scattering [23]. According to papers [18,19], if after interaction with a phonon $\hbar\Omega$ an electron of energy ε obtains energy ε' where $\varepsilon' = \varepsilon + \hbar\Omega$, the expression for the spectral distribution function can be approximated as

$$\alpha^2F(\varepsilon,\varepsilon',\Omega) = \left[\frac{N(\varepsilon)N(\varepsilon')}{N^2(E_F)}\right]\alpha^2F(\Omega) \approx \left[\frac{N^2(\varepsilon)}{N^2(E_F)}\right]\alpha^2F(\Omega), \quad (2)$$

where $\alpha^2F(\Omega) \equiv \alpha^2F(E_F, E_F, \Omega)$. Here we use the assumption that the electron-phonon matrix element is independent of the initial and final electron states $\{\mathbf{k}, i\}$ and $\{\mathbf{k}', j\}$ [18,19].

In order to improve the calculation accuracy of α^2F, we refuse approximation (2) and directly take into account the variation of the electron-phonon scattering matrix with the increasing electron temperature, however keeping within Allen's formalism [23]. Consider a crystal with a density ρ and an electron temperature T_e. Like in Ref. [24], define the electron-phonon spectral function for specified electron energy ε as

$$\alpha^2F(\varepsilon,\Omega) = \frac{2}{\hbar N(\varepsilon)} \sum_{\mathbf{q},\nu} \delta(\Omega - \omega_{\mathbf{q},\nu}) \sum_{\mathbf{k},i,j} \left|g^{\mathbf{q},\nu}_{\mathbf{k}+\mathbf{q},j;\mathbf{k},i}\right|^2 \times \delta(\varepsilon_{\mathbf{k},i} - \varepsilon)\delta(\varepsilon_{\mathbf{k}+\mathbf{q},j} - \varepsilon). \quad (3)$$

Here we use the following reasonable approximation. Since the scale of electron energy variation is much greater than that of phonon energies, we can omit the term $\hbar\Omega$ and write $\alpha^2F(\varepsilon, \varepsilon + \hbar\Omega, \Omega) \approx \alpha^2F(\varepsilon, \varepsilon, \Omega) \equiv \alpha^2F(\varepsilon, \Omega)$ [19,23]. In Eq. (3), $g^{\mathbf{q},\nu}_{\mathbf{k}+\mathbf{q},j;\mathbf{k},i}$ is the electron-phonon matrix element which defines the probability of electron scattering from the initial state $\{\mathbf{k}, i\}$ into the final state $\{\mathbf{k}', j\}$ by a phonon $\{\mathbf{q}, \nu\}$ with frequency $\omega_{\mathbf{q},\nu}$. The factor 2 accounts for spin polarization. The way in which the electron-phonon matrix element is computed depends on the particular implementation of the *ab initio* method. For more details on its implementation in the case of the full-potential LMTO method, see Ref. [25], and for the pseudopotential method (Quantum ESPRESSO code), see Ref. [26].

Using function (3), we can write the rate of energy transfer from the electrons to the lattice per unit volume in the form

$$\frac{\partial E_e}{\partial t} = 2\pi \int_0^\infty \hbar\Omega d\Omega \int_{-\infty}^\infty N(\varepsilon)\alpha^2F(\varepsilon,\Omega)S(\varepsilon,\varepsilon+\hbar\Omega)d\varepsilon, \quad (4)$$

where $S(\varepsilon, \varepsilon + \hbar\Omega) = [f_e(\varepsilon) - f_e(\varepsilon + \hbar\Omega)][n(\hbar\Omega, T_l) - n(\hbar\Omega, T_e)]$ [19], $n(\hbar\Omega, T)$ denotes the Bose-Einstein distribution function, and T_l is the lattice temperature. It is easily seen that at low temperatures, integration with respect to electronic energy is limited to only the electrons which are on the Fermi level and formula (4) becomes identical to formula (10) from Allen's paper [23].

Now, using the two-temperature model representation [14,27] for the energy exchange rate, $\partial E_e/\partial t = G(T_e)(T_l - T_e)$, express the electron-phonon coupling factor as

$$G(T_e) = \frac{2\pi\hbar}{(T_l - T_e)} \int_0^\infty \Omega d\Omega \int_{-\infty}^\infty N(\varepsilon)\alpha^2F(\varepsilon,\Omega) \times S(\varepsilon,\varepsilon+\hbar\Omega)d\varepsilon. \quad (5)$$

If we use some simplifying approximations for the function S, as the authors of Ref. [19], we can rewrite Eq. (5) in the form

$$G(T_e) = 2\pi\hbar k_B \int_0^\infty \Omega d\Omega \int_{-\infty}^\infty N(\varepsilon)\alpha^2F(\varepsilon,\Omega)\left(-\frac{\partial f_e}{\partial\varepsilon}\right)d\varepsilon. \quad (6)$$

Spectral distribution function Eq. (3) and the other quantities defined by Eqs. (4)–(6) can be calculated from first principles for each value of density ρ and electron temperature T_e, using the electron and phonon spectra defined for these particular conditions. These calculations can quite easily be built into the available codes which implement the calculation of $\alpha^2F(\Omega) = \alpha^2F(E_F, E_F, \Omega)$. In our case, it is necessary to determine α^2F not only for $\varepsilon = E_F$, but for ε within a certain range of interest, whose boundaries are defined by the Fermi-Dirac distribution. Then we can do double integration with standard methods and calculate the required physical quantity. Thus we succeed to rather accurately calculate $\alpha^2F(\varepsilon, \Omega)$ for

specified (ρ, T_e) and determine the temperature dependence $G(T_e)$.

Our calculations show that the values of G determined by Eqs. (5) and (6) may differ by 15% due to the substitution of $(-\partial f_e/\partial\varepsilon)$ for the function S. But such a difference is only present at low temperatures and at $T_e > 1000$ K it rapidly reduces to become no higher than 1% which agrees well with results from Ref. [19]. Later on we define the electron-phonon coupling factor using Eq. (5). Comparison with available experimental data and other calculations for Cu, Au, and Pt are provided below in Sec. III.

B. Details of first-principles calculations

For predicting the properties of copper, gold, and platinum from first principles, we use the all-electron full-potential linear muffin-tin orbital (FP-LMTO) method [28] which has proved to perform well for materials under pressure (see, for example, Refs. [29,30]). Within density functional theory, the FP-LMTO method allows us to calculate the internal energy (and some related quantities such as the phonon spectrum, the electron-phonon spectral function, etc.) of the electron subsystem in the external field of fixed nuclei for different electron temperatures and material densities. The valence electrons in our calculations are $3s$, $3p$, $3d$, and $4s$ for Cu; $5s$, $5p$, $4f$, $5d$, and $6s$ for Au; and $5s$, $5p$, $4f$, and $5d$ for Pt. The electronic population is defined by the Fermi-Dirac distribution function. Entropy of the electron subsystem for specified ρ is determined by

$$S_e(T_e) = -k_B \int_{-\infty}^{\infty} N(\varepsilon)[f_e \ln(f_e) + (1-f_e)\ln(1-f_e)]d\varepsilon, \tag{7}$$

where $N(\varepsilon)$ is a T_e-dependent electron DOS. The electron heat capacity is calculated as

$$C_e(T_e) = T_e\left[\frac{\partial S_e(T_e)}{\partial T_e}\right]_\rho. \tag{8}$$

The phonon spectra are obtained from linear response theory implemented in the FP-LMTO code [28]. After determining the phonon spectrum of the lattice, we can calculate its heat capacity in quasiharmonic approximation by the well-known formula [31]

$$C_l(T_l) = k_B V \int_0^\infty F(\Omega)\left(\frac{\hbar\Omega}{2k_BT_l}\right)^2 \sinh^{-2}\left(\frac{\hbar\Omega}{2k_BT_l}\right)d\Omega, \tag{9}$$

where $F(\Omega)$ is a T_e-dependent phonon DOS, and V is a specific volume. Our calculations for different T_e suggest that $C_l(T_l)$ is weakly dependent on electron temperature. Therefore, for calculations by the two-temperature model we use $C_l(T_l)$ defined at $T_e = 300$ K. At high T_l, the lattice heat capacity almost perfectly agrees with the classical limit $3R$.

In order to determine the temporal evolution of electron and lattice temperatures after ultrashort laser irradiation, we use the two-temperature model equations [14]

$$C_e(T_e)\frac{\partial T_e}{\partial t} = -G(T_e)(T_e - T_l) + S(t), \tag{10}$$

$$C_l(T_l)\frac{\partial T_l}{\partial t} = G(T_e)(T_e - T_l). \tag{11}$$

Here $S(t)$ is a Gaussian-shaped source term [32]. Equations (10) and (11) neglect lattice heat conductivity because it is negligible compared to electron heat conductivity in metals. Also omitted is the term with electron heat conductivity since we consider the irradiation regime where ballistic electrons quickly (during $t \sim \tau_p$) equilibrate the electronic subsystem with no significant temperature gradients in the target [8,9].

The temporal evolution of the relative diffraction peak intensity was calculated from

$$I(t)/I_0 = \exp\left(-\left[\langle u^2\rangle(t) - \langle u_0^2\rangle\right]Q^2/3\right), \tag{12}$$

$$\langle u^2\rangle = \frac{\hbar V}{2M}\int_0^\infty \frac{F(\Omega)}{\Omega}\coth\left(\frac{\hbar\Omega}{2k_BT_l}\right)d\Omega. \tag{13}$$

Here $\langle u^2\rangle$ is the mean-square displacement (MSD) of an atom from the equilibrium position ($\langle u_0^2\rangle$ is MSD at room temperature), M is the atomic mass, and Q is the scattering vector. For the convenience of comparison between various calculations and experiments, from the values of $\langle u^2\rangle$ we define the T_e-dependent Debye temperature $\Theta_D(T_e)$ (at $T_l =$ 300 K) using the equation

$$\langle u^2\rangle = \frac{9\hbar^2}{Mk_B\Theta_D(T_e)} \times\left[\frac{1}{4} + \left(\frac{T_l}{\Theta_D(T_e)}\right)^2\int_0^{\Theta_D/T_l}\frac{x}{\exp(x)-1}dx\right]. \tag{14}$$

The resulted Debye temperatures are in good agreement with available experimental data and data from other calculations (within 5%). Some comparisons will be demonstrated below.

To determine the time when the considered metals melt after laser irradiation, we calculate the melting temperature T_m as a function of T_e, as it is done in Ref. [12], with the use of the Lindemann criterion and calculated phonon spectra. As shown, for example, in papers [12,29], in this manner it is possible to reproduce well the melting curve of metals, specifically copper and gold, under pressure. In this work we also do a comparison for platinum under pressure. Calculating from Eqs. (10) and (11) how electron and lattice temperatures depend on t, we can determine the time when T_l reaches the melting point for different absorbed energy densities and compare the resulted times with experiment.

To attain high accuracy of *ab initio* calculations, a thorough selection of the FP-LMTO internal parameters was carried out, first of all, the exchange-correlation (XC) functional. The criterion for its choice was its ability to better reproduce the ground state properties and phonon spectra for the three metals of interest. So we took the XC functional [34] with gradient corrections [35] for copper, the local functional [36] for gold, and PBEsol [37] XC was found most appropriate for platinum. The XC functionals we took for Cu and Au have proved to perform well in our earlier calculations [29,38].

The integration over the Brillouin zone was performed with the improved tetrahedron method [39]. The mesh in $\mathbf{k}$ space was taken to be $40 \times 40 \times 40$ for all metals under consideration. As shown by our calculations, such dense meshes are necessary for determining the electron-phonon

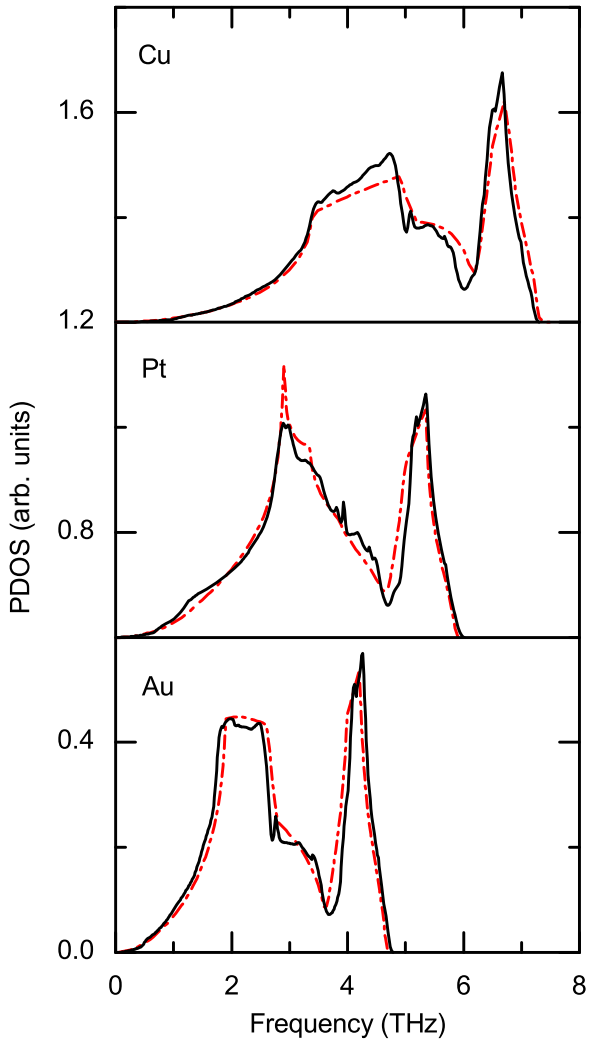

FIG. 1. Phonon DOS calculated in this work (solid lines) in comparison with experiment [33] (dashed-dotted lines) for Cu, Au, and Pt. Densities correspond to ambient conditions.

coupling factor more accurately. If the number of points is smaller than $30 \times 30 \times 30$, the error of the calculated $G(T_e)$ may be twice as high. A $10 \times 10 \times 10$ mesh was found quite sufficient for integrating the phonon spectrum over $\mathbf{q}$ points. To illustrate the accuracy of phonon calculation we compared our calculated phonon densities of states (PDOS) with available experimental data for the three metals. Figure 1 shows the result of our comparison. As seen from Fig. 1, the obtained curves agree quite well with experiment.

The energy cutoff for representing the basis functions as a set of plane waves in the interstitial region was taken to be 800 eV. The basis set was restricted to orbital moment $l^b_{\max} = 5$. The spherical harmonic expansion of charge density and potential was done to moment $l^w_{\max} = 7$. The values for such FP-LMTO parameters as linearization energies, tail energies, and the MT-sphere radius R_{MT} were selected with an approach similar to that described in Ref. [29]. Our calculations were done for densities ρ_0 corresponding to the densities of the considered metals under ambient conditions unless otherwise stated.

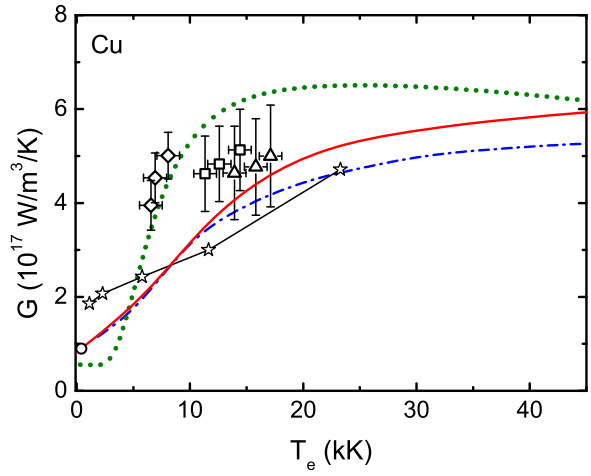

FIG. 2. Electron-phonon coupling factor as a function of electron temperature T_e. The lines demonstrate various calculations: Solid line (our calculation), dash-dotted line [40], dotted line [19], stars connected with lines [41] for molten Cu with solid density ρ_0. The circle experiment [42]; diamonds, squares, and triangles experiment [21].

III. RESULTS

A. Copper

Consider copper for which are available quite many results on $G(T_e)$, both calculated [19,40,41] and experimental [21,42,43]. Figure 2 compares different calculations and experiments. The value of G we determined at room temperature very well agrees with experimental data [42,43]. So the authors of paper [42] analyzed how the intensities of different diffraction peaks changed after irradiation of femtosecond pulses and found G to be equal to $(0.9 \pm 0.1) \times 10^{17}$ W/m^3 K^{-1}. Our calculations gave the same quantity. Another theoretical work [40] also reports a close value of the electron-phonon coupling factor. The value determined in Ref. [19] for $G(T_e = 300\ \mathrm{K})$ is noticeably lower and equals 0.56×10^{17} W/m^3 K^{-1}. Such an underestimation is due to, first, the replacement of the function S for the derivative $(-\partial f_e/\partial \varepsilon)$ [formulas (5) and (6)], which, as mentioned above, affects the result. Second, the authors of Ref. [19] do their calculations with an underestimated value of $\lambda\langle\omega^2\rangle$ taken from [44]. Borson *et al.* [44] extracted the $\lambda\langle\omega^2\rangle$ from the measurements of the reflectivity of copper after femtosecond laser irradiation, using the two-temperature model. They obtained the value 29 meV^2, while in our calculations $\lambda\langle\omega^2\rangle = 57$ meV^2 which gives a much better agreement with the measured value of G [42,43].

As seen from Fig. 2, the curves $G(T_e)$ from our calculation and from Ref. [40] agree quite well. It is because the authors of paper [40] determine G using the earlier analog of formula (4) [23,27]. The details of their approach are described in Ref. [45]. It should only be noted that for solving the equation which determines the electron-phonon energy exchange rate, the authors of work [45] make a number of simplifying assumptions. The main one is the approximate treatment of the interaction potential and the probability of electron transition from one state into another. Despite these

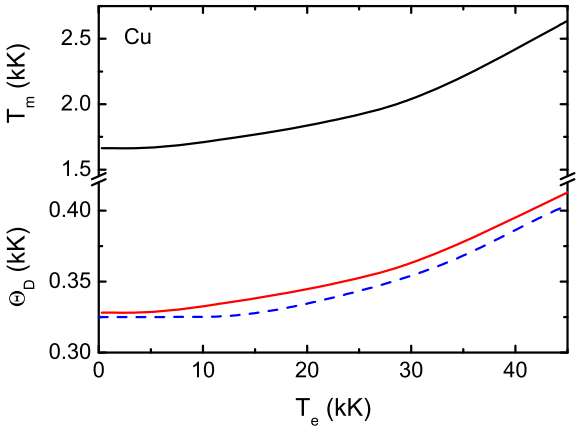

FIG. 3. Melting temperature and Debye temperature versus electron temperature for copper from our calculations (solid lines). Dashed line Θ_D from calculations [46].

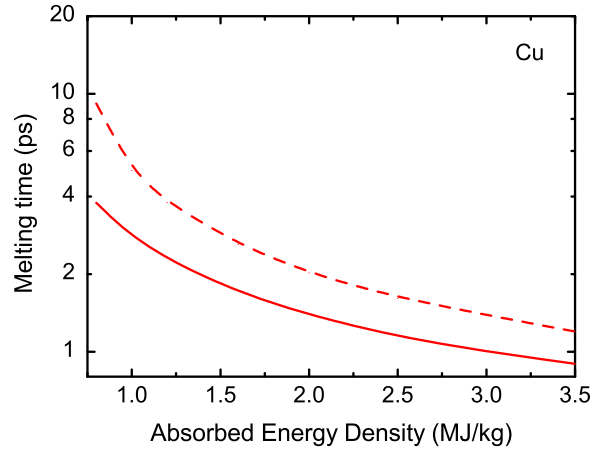

FIG. 4. Melting time versus absorbed energy density for copper from calculations with no account for the latent heat (solid line) and with its account (dashed line).

important simplifications, for copper the approach [45] gives a good agreement with our calculation which was done without the above approximations. The curve of Lin and Zhigilei [19] rises more sharply in the temperature range from ∼4 to 10 kK (Fig. 2) and, on the whole, varies with the increasing temperature stronger than our curve thus overestimating the values of $G(T_e)$.

A rather good agreement is also observed with the experimental results reported in Ref. [21], where a thin copper film was isochorically heated by femtosecond laser pulses, and using x-ray absorption near edge spectroscopy, the authors managed to retrieve the values of the electron-ion coupling factor for warm dense copper. Though Cu in their experiment [21], as we will show below, was very likely in a liquid state, our results are not contradicting the measurements. Figure 2 also shows data from paper [41] for liquid copper at the solid density, which were calculated from first principles within Kubo formalism. They agree rather well with our calculations and data from Ref. [40] at $T_e > 5$ kK. Noticeable disagreement with experiment [21] between 5 and 10 kK requires further research both experimental and theoretical.

In order to better understand in which solid or liquid state copper was under experimental conditions [21], we calculated the melting curve $T_m(T_e)$ from the Lindemann criterion [12] on the isochore for the solid density. Figure 3 shows the dependence we obtained along with the curve $\Theta_D(T_e)$. It is seen that T_m increases as the electron temperature grows, i.e., like in the case of gold [10], the copper lattice hardens. It is caused by the depopulation of occupied $3d$ bands with the increasing T_e, which reduces the screening of the Coulomb potential of nuclei and makes the ion-ion interaction potential more rigid [10,38]. This behavior agrees well with other *ab initio* calculations [12,46].

If we then calculate by Eqs. (10) and (11) the temporal evolution of T_e and T_l, we can determine the time when the lattice temperature reaches T_m on the melting curve (Fig. 3). Figure 4 shows how this time depends on absorbed energy density E_{abs} (solid line). The curve itself does not point to lattice melting because it is also necessary to consider latent heat ΔH_m. Its value is known from experiments at zero pressure [47]. Note that the value of ΔH_m may markedly differ when matter is under the external action of, for example, compression [48]. But here we can do a simple estimation by using data from Ref. [47]. After reaching the melting temperature, the amount of heat received by the lattice from electrons can be estimated from the expression

$$\Delta E_m = \frac{1}{\rho}\int_{t_{\text{melt}}}^{t_f} G(T_e)(T_e - T_l)dt. \tag{15}$$

Here t_{melt} is the time when the lattice temperature reaches melting temperature at $T_m(T_e)$ curve, and t_f is the time when ΔE_m becomes equal to ΔH_m. The dashed line in Fig. 4 shows how t_f varies with the growth of absorbed energy density E_{abs}. The line roughly determines the time when the lattice gets enough heat for melting.

It is seen from Fig. 4 that at low E_{abs} the time t_f may be several times greater than t_{melt}. With the increasing absorbed energy density the difference quickly reduces to about 20%–25% for the considered interval of E_{abs}. At $E_{\text{abs}} = 3.5$ MJ/kg, the time of copper melting is shorter than 2 ps (Fig. 4) due to the high electron-phonon coupling factor and absorbed energy. Even if latent heat is twice as high as the reference value [47], melting will have completed by $t \approx 1.5$ ps. The minimal value of absorbed energy density in experiments [21] was 3.5 MJ/kg and therefore it is very likely that the measurements at 2 ps and later corresponded to the liquid state of Cu. A more detailed comparison of the calculated melting time with experiments requires additional measurements like it is done for gold [4,7].

Experiments [21] also give a number of interesting physical quantities which can be compared with calculations. In spite of what was stated above, we will try to understand whether the difference between the solid and liquid states is essential for the experimentally measured quantities provided below. Figure 5 shows T_e-dependent electron heat capacities from different calculations for crystal copper and the experimentally determined C_e. The differences we can see in the curves $C_e(T_e)$ at high temperatures can be attributed to differences between the exchange-correlation functionals [49]. On the whole, the calculated dependencies agree well

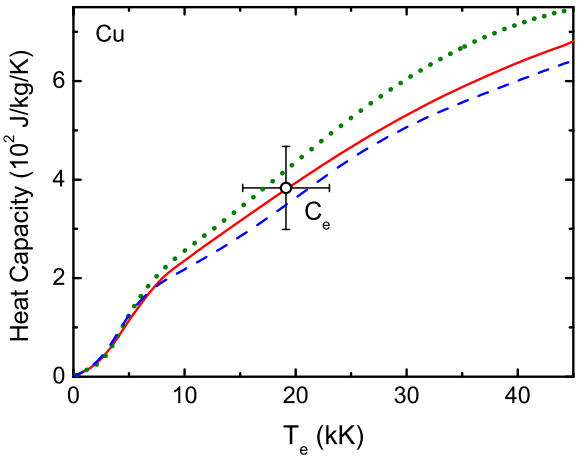

FIG. 5. Electron heat capacity as a function of temperature T_e for Cu from our calculations (solid line), and from other calculations: Dotted line [19] and dashed line [49]. Open circle is the experimental value [21].

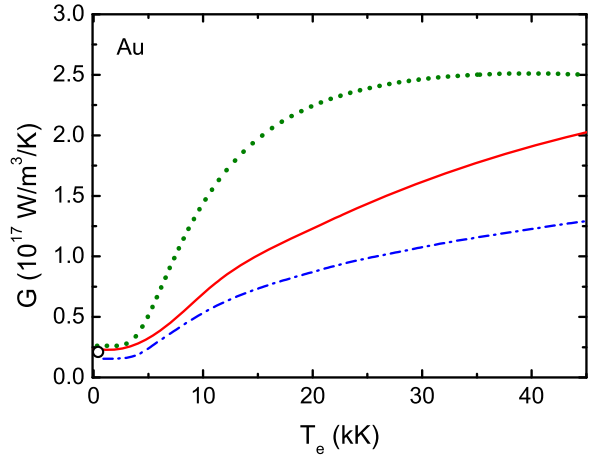

FIG. 7. Electron-phonon coupling factor versus electron temperature T_e for gold from our calculation (solid line), and other calculations: Dashed-dotted line [45] and dotted line [19]. Open circle is the experiment [8].

with experiment. As earlier shown in Ref. [50], $C_e(T_e)$ is weakly dependent on the lattice type and can be described quite well even by the average atom model.

By determining the temporal evolution of electron and lattice temperatures from the solution of two-temperature model equations (10) and (11), we can obtain how the initial (the peak value of T_e) and final ($T_e = T_l$) temperatures depend on absorbed energy density. Figure 6 compares our calculations with experimental and calculated results from paper [21] where $G(T_e)$ was determined from formula (1), and the electron heat capacity and electron-phonon coupling factor were calculated with the electron DOS for liquid copper with solid density. It is seen from Fig. 6 that our results agree quite well with experiment. Also, they excellently agree with calculations [21]. In this case, the utilization of the liquid DOS for the determination of $C_e(T_e)$ and $G(T_e)$ is almost of no effect on the shape of the curve $T_e(E_{\rm abs})$ compared to our results obtained for the solid state.

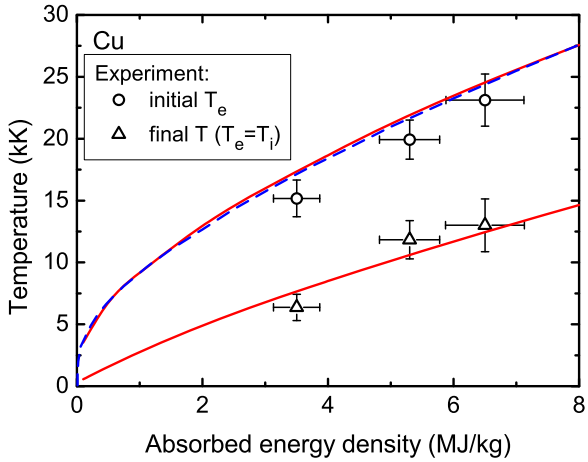

FIG. 6. Initial and final electron temperatures versus absorbed energy density from experiment [21] (circles and triangles, respectively), and from our calculation (solid lines) and calculation [21] (dashed line) for liquid copper with solid density.

B. Gold

Gold is a metal which is currently an object of intensive research both theoretical and experimental (see, for example, [4,7–11,13,15]). Here we will focus on the electron-phonon coupling and melting of its thin films after irradiation to femtosecond laser pulses. Figure 7 shows the function $G(T_e)$ for Au. Unfortunately, the experiment gives us its value only for low temperatures. The result of our calculation, $G = 2.3 \times 10^{16}$ W/m^3 K^{-1}, agrees well with its experimental value $(2.1 \pm 0.3) \times 10^{16}$ W/m^3 K^{-1} [8]. Other calculations [19,45] also give rather close values.

The gold electron-phonon coupling factor is seen (Fig. 7) to markedly increase as T_e grows. As in the case of Cu, calculations from paper [19] noticeably overestimate the rise of function $G(T_e)$. On the other hand, the approximated approach [45] (we use here the curve $m_s/m = 1$) gives lower values compared to our results. Therefore, we can use the curves from Refs. [19,45] as upper and lower bounds for possible deviations of $G(T_e)$ and see how this reflects on results of calculations below.

Figure 8 presents $\Theta_D(T_e)$ and $T_m(T_e)$ we calculated on the isochore ρ_0 and the Debye temperature calculated in paper [10]. Our curve $\Theta_D(T_e)$ is seen to agree quite well with results provided by Recoules *et al.* [10]. As seen from Fig. 8, the crystal lattice hardens at high T_e, however, the values of T_m and Θ_D remain almost constant to temperatures $\lesssim$15 kK. This means that we should search for the experimental evidence of gold hardening after irradiation by laser pulses at much higher electron temperatures (above 25 kK [13]).

Now compare the temporal evolution of (220) diffraction peak intensity after irradiation of a free-standing gold film by the laser pulse from our calculation with experiments reported in Refs. [4,7]. Though the experiments slightly differ in their conditions (pump pulse duration and target thickness), they complement each other rather well. Figure 9 compares exper-

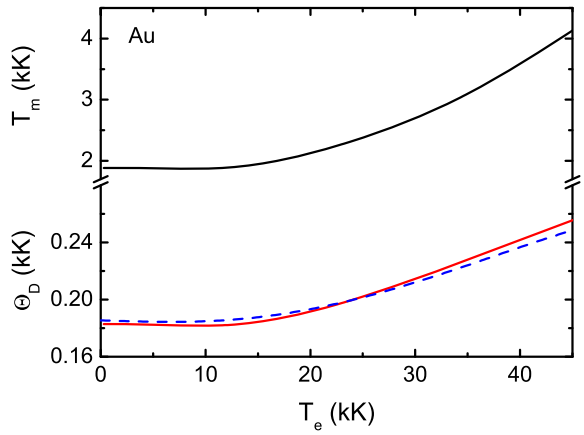

FIG. 8. Melting temperature and Debye temperature as a function of electron temperature for gold from our calculation (solid lines). Dashed line: Calculation of Θ_D from Ref. [10].

imental data with our results obtained for different calculation parameters. The red solid line C1 shows our calculation of $G(T_e)$, $C_e(T_e)$, and $\Theta_D(T_e)$ determined by formulas (5), (8), (13), and (14), respectively. The blue solid line C2 shows calculation with the same parameters but the electron-phonon coupling factor was taken from Ref. [45]. The curve C3 is $G(T_e)$ from paper [19] and the constant Debye temperature. Since $\Theta_D(T_e)$ remains almost unchanged up to $T_e \sim 15$ kK (see Fig. 8), it is quite reasonable to use for absorbed energy densities below ~1.2 MJ/kg the constant value $\Theta_D = 183$ K we determined in this work. This assumption is almost of no effect on calculation accuracy. As seen from Figs. 9(a)–9(d), the use of formula (5) for the determination of $G(T_e)$ (curve C1) makes an agreement between calculation and experiment much better compared to the function by Lin and Zhigilei (curve C2) [19]. Curve C2 runs markedly lower because of the overestimated electron-phonon coupling factors at elevating electron temperatures.

The noticeable difference between the calculated curve C1 and experimental data at low absorbed energy densities (<1 MJ/kg) and $t > 16$ ps comes clearly from the fact that our calculations do not consider the effect of target expansion at large times. But if we reduce material density to $\rho = \rho_m$, where ρ_m is the density at which gold starts to melt under ambient pressure ($P = 0$) [52], then our results for $t > 16$ ps agree with experiment much better. So, for $E_{\text{abs}} = 0.36$ MJ/kg at $t = 21$ ps, the normalized intensity is calculated to be 0.2 which is in good agreement with the experimental value 0.15 ± 0.07 [7]. This effect is attained due to, first of all, the much lower Debye temperature which at $\rho = \rho_m$ equals 153 K against 183 K at ρ_0. At high absorbed energy densities [$E_{\text{abs}} > 1$ MJ/kg, Figs. 9(c)–9(f)], we do not observe

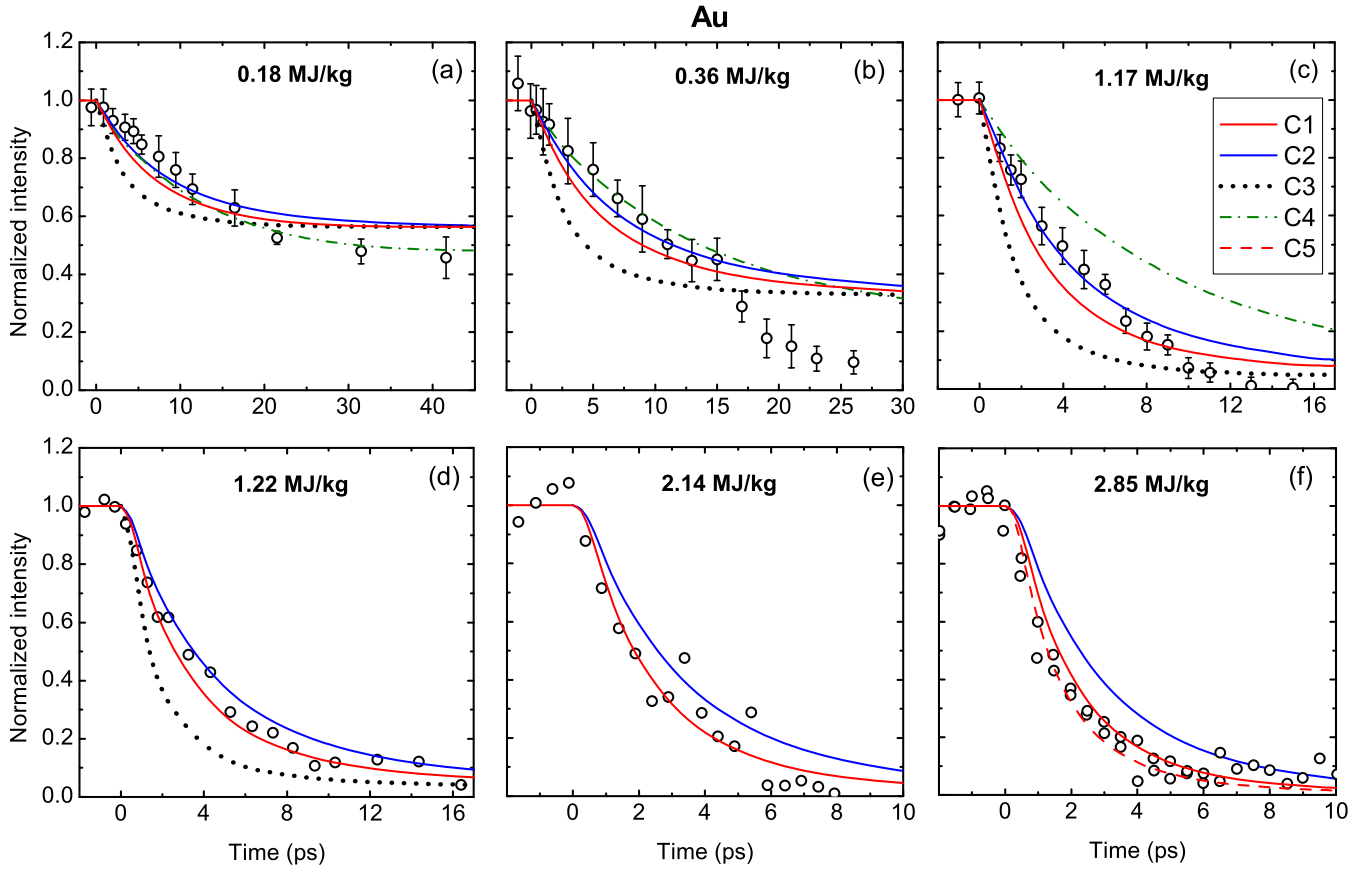

FIG. 9. Temporal evolution of (220) diffraction peak intensity from experiments (circles) [7] (top figures) and [4] (bottom figures) and calculations: Curve C1 obtained using $G(T_e)$ calculations by formula (5) and $\Theta_D(T_e)$ by formulas (13) and (14); C2 $G(T_e)$ from [45] and $\Theta_D(T_e)$ by formulas (13) and (14); C3 $G(T_e)$ from [19] and $\Theta_D = \text{const.}$; C4 $G = \text{const.}$, $\Theta_D = \text{const.}$, and $C_e = \gamma T_e$ [51]; C5 $G(T_e)$ from formula (5) and $\Theta_D = \text{const.}$ (see the text for details).

any substantial effect of target expansion. It is not unlikely that under these conditions at times <15 ps the lattice is not much expanded and the situation is similar to experiment [2] for aluminum where no significant lattice expansion was observed. The curve C2 in Fig. 9 at $E_{\rm abs} < 1.2$ MJ/kg and $t < 16$ ps agrees with experiments even a bit better than C1. However, the agreement becomes worthy as absorbed energy density increases [Figs. 9(e) and 9(f)].

The effect of lattice hardening can be seen in Fig. 9(f) at $E_{\rm abs} = 2.85$ MJ/kg. Here the peak electron temperature equal to about 27.5 kK is the highest. The curve C5, unlike C1, is calculated for constant $\Theta_D = 183$ K. It is seen that within the experimental error it is not possible to confirm lattice hardening with certainty. Moreover, our calculations show that the difference between the curves C1 and C5 remains quite small as $E_{\rm abs}$ increases.

Figures 9(a)–9(c) also show a curve from our calculation we did for the conditions of molecular dynamics research [51], where the value of G was taken to be constant and equal to 2.1×10^{16} W/m^3 K^{-1}, and the electron heat capacity was a linear function of temperature $C_e = \gamma T_e$. Calculations in Ref. [51] were done for rather low absorbed energy densities $E_{\rm abs} < 0.5$ MJ/kg. If we use the above parameters of the two-temperature calculation and take $\Theta_D = 183$ K, the results quite adequately reproduce experiment [7] for low $E_{\rm abs}$ [Figs. 9(a) and 9(b)]. But for high $E_{\rm abs}$ we see the decay of the (220) diffraction peak intensity to be significantly underestimated [Fig. 9(c)]. This is quite explainable because the calculation parameters we specify tend to underrate the values G and C_e with the increasing electron temperature [19]. At low $E_{\rm abs}$ these underestimations compensate each other. But this compensation is disabled as absorbed energy densities become higher. It should be noted that MD calculations take into account the expansion of the target and hence can better reproduce experimental results at longer observation times ($t > 15$ ps) than our calculations.

Below we consider the dependence of melting time on absorbed energy density for a gold film. Figure 10 shows this dependence we calculated with and without latent heat in comparison with experimental data [4,7,53] and other calculations [13,32,51]. Our calculations were done for the values of $G(T_e)$ and C_e determined with formulas (5) and (8). The experimental points [7] refer to the totally melted target (triangles for single crystal and circles for polycrystal). Points from paper [4] (polycrystal) show the decay of the (220) diffraction peak (squares), the start of diffusion scattering (diamonds), and the rise of the diffraction peak typical for a liquid (circles). The experimental value from Ref. [53] marks the formation of the diffraction pattern similar to liquid. As mentioned above, the use of results from MD calculations [51] for low $E_{\rm abs}$ is quite appropriate despite that calculation parameters are not quite adequate. The same can be told about results from [32] where values for G and $C_e(T_e)$ were chosen in a similar way. Several points from those calculations are also shown in Fig. 10. They correspond to the totally melted Au target.

It is seen from Fig. 10 that like in the case of copper, accounting for ΔH_m makes the melting time of gold much longer when absorbed energy densities are low ($E_{\rm abs} < 1$ MJ/kg). But already for $E_{\rm abs} > 1$ MJ/kg, the effect

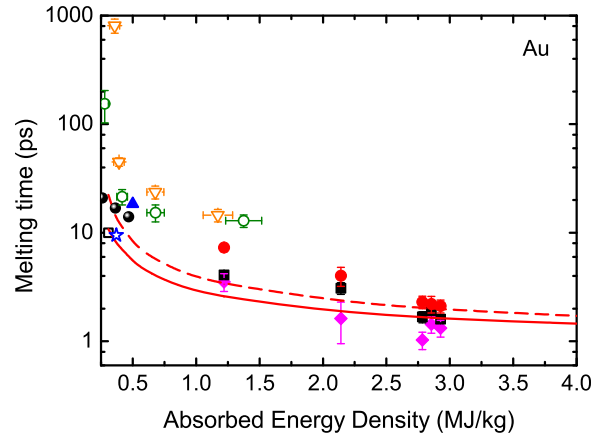

FIG. 10. Melting time versus absorbed energy density for gold. Solid and dashed lines (our calculations) with no account for the latent heat and with its account, respectively. MD simulations: Black circles [51], blue star [13], and blue triangle [32]. Experimental data: Open orange triangles and green circles experiments [7], closed red circles, black squares, and violet diamonds [4], open square [53] (see the text for details).

becomes much weaker. The melting time begins to drop much slower as absorbed energy density increases and reduces by less than 1 ps in the interval from 2 to 4 MJ/kg. Our results agree very well with experimental data [4] for absorbed energy densities >2.5 MJ/kg. For lower $E_{\rm abs}$, the agreement is reasonable. Despite that our results are only an estimation, we see that for low $E_{\rm abs}$ they agree quite well with MD calculations from papers [13,32,51]. The authors of Ref. [13] determined $G(T_e)$ from formula (1) and hence overestimated it thus reducing a bit their melting time compared to other calculations. Further MD calculations at higher $E_{\rm abs}$ (>0.5 MJ/kg) are needed in order to better understand the behavior of melting time versus absorbed energy density. It would be also interesting to see how latent heat changes in a material heated to a nonequilibrium state. New experimental data for intermediate $E_{\rm abs}$ from 1.5 to 2.5 MJ/kg and above 3 MJ/kg would be also helpful. Special attention should be given to the quality of films because defects in it can strongly affect measurement results [54].

C. Platinum

Platinum is the least studied metal among those we are considering. Its electronic structure differs from those of Cu and Au [19]. Electron density of states for Pt on the Fermi level is much higher due to 5d electrons than in the other considered metals. Its chemical potential increases as the electron temperature grows, which drastically reduces DOS in its vicinity and lowers the contribution of 5d electrons to the electron-phonon coupling [19]. Figure 11 demonstrates how the electron-phonon coupling factor varies with the increasing electron temperature by data from our calculation in comparison with experiments [8,55] and calculations [19]. The experimental values of G are seen to greatly differ. Such a difference is also typical of another metal in this group, nickel [19]. At relatively low temperatures the value of G for platinum sharply changes (Fig. 11) and this may increase the

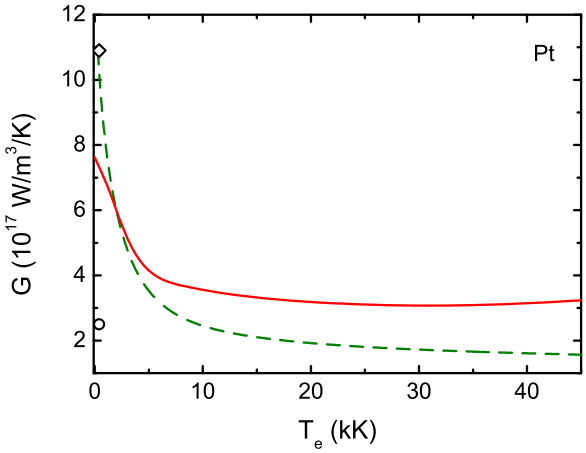

FIG. 11. Electron-phonon coupling factor as a function of T_e for platinum from our calculation (the solid line), calculations [19] (dashed line), and experiments [8] (circle) and [55] (diamond).

error of its experimental determination. Further experimental studies, similar to Ref. [42], could be very useful for determining the value of the electron-phonon coupling factor of Pt more accurately. The value $G = 7.4 \times 10^{17}$ W/m^3 K^{-1} we obtained in our calculation at room T_e is closer to the results of experiment [55]. The curve obtained in paper [19] drops sharper than in our calculation (Fig. 11). After a rather sharp decrease at relatively low temperatures ($T_e \lesssim 7$ kK), the electron-phonon coupling factor of platinum changes weakly to at least $T_e = 45$ kK and can be considered as almost constant.

Then, in order to be sure in the accuracy of our calculation of the melting temperature for Pt, we calculated the dependence of T_m on pressure under equilibrium heating. Figure 12 shows the results we obtained in comparison with recent experiments and other calculations. Our curve is seen to agree quite well with *ab initio* molecular dynamics calculations [56,57] and experimental data [57,58]. The Lindemann

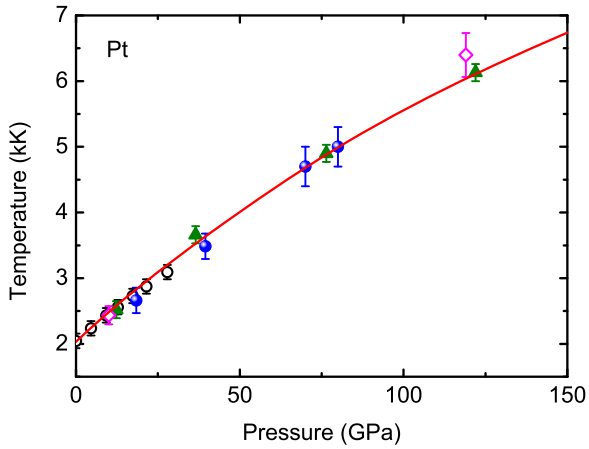

FIG. 12. Melting temperature versus pressure for platinum from our calculation (solid red line) and *ab initio* MD calculations [56] (diamonds) and [57] (triangles). Closed and open circles experiments [57,58].

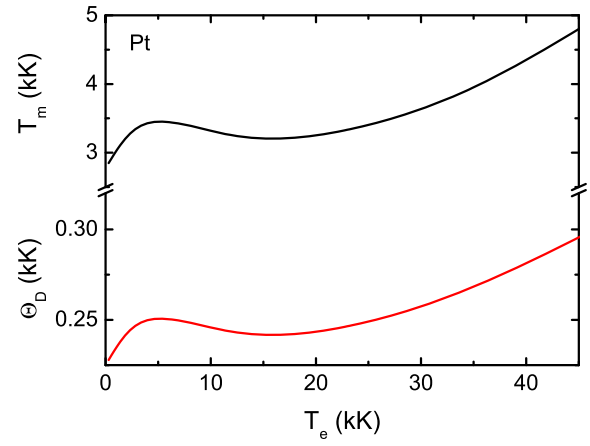

FIG. 13. Melting temperature and Debye temperature versus electron temperature for platinum.

criterion adequately reproduces T_m versus pressure for Pt and we will use it further for determining $T_m(T_e)$.

Figure 13 shows the resulted $T_m(T_e)$ and $\Theta_D(T_e)$. The value $\Theta_D = 228$ K we determined at room temperature agrees well with the experimental value $\Theta_D = 225$ K [59]. The curves are clearly seen (Fig. 13) to increase at $0.3 < T_e < 5$ kK. This hardening of the lattice is likely to be also caused by the change of the chemical potential and the sharp reduction of the d-electron DOS in its vicinity with the increasing temperature [19]. After that the values slightly decrease and then begin to grow again and the behavior of the curves becomes similar to that of the other considered metal. The same behavior of the melting curve is observed for nickel [12]—a metal which has a similar electronic structure as platinum.

Figure 14 shows melting time versus absorbed energy density from our calculation. On the whole, the behavior of melting time is similar to other metals. The melting temperature of Pt at zero pressure is higher compared to Cu and Au, but its factor G is much bigger at relatively low temperatures. At $E_{\text{abs}} \leqslant 0.5$ MJ/kg its melting time is quite long and exceeds 20 ps. The time of lattice disordering strongly reduces with the

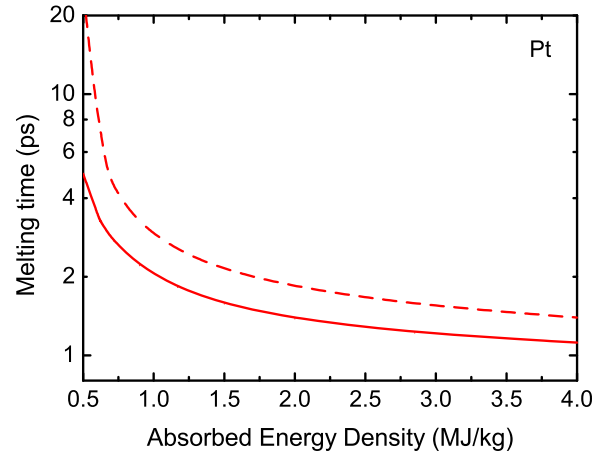

FIG. 14. Melting time versus absorbed energy density for platinum from our calculation with no account for latent heat (solid line) and with its account (dashed line).

increasing absorbed energy density and will be less than 10 ps at $E_{\rm abs} > 0.75$ MJ/kg. However, at least to energies about 4 MJ/kg melting proceeds on the picosecond time scale. This behavior is also similar to what was obtained for copper and gold.

IV. CONCLUSIONS

We have studied the interaction of femtosecond laser pulses with the thin films of copper, gold, and platinum. We proposed an improved approach to determining the temperature evolution of the electron-phonon coupling factor $G(T_e)$ from first principles in order to more accurately describe the processes governing the transfer of energy from hot electrons to the relatively cold lattice. We compared the values of G calculated for Cu, Au, and Pt with available experimental data and other calculated results for electron temperatures from 300 K to 45 kK and showed that the formula from Refs. [18,19] overestimated (up to a factor of 2) the scale of changes in G in this temperature range. Our comparisons for copper shows that at $T_e > 5$ kK the difference between the values of G for liquid and solid phases does not exceed 20%. The approach we propose for determining $G(T_e)$ can rather easily be implemented in codes which already can calculate the electron-phonon spectral distribution function $\alpha^2F(\Omega)$.

For three metals we estimated the melting time of their thin films as a function of absorbed energy density. The calculated melting times are shown to significantly depend on the latent heat when absorbed energy densities are rather small, $E_{\rm abs} < 1$ MJ/kg. For higher values of $E_{\rm abs}$, the effect strongly reduces. Comparison with experimental data on the decay of (220) diffraction peak intensity with time for gold after femtosecond irradiation shows that at $E_{\rm abs} \gtrsim 1.2$ MJ/kg, in all likelihood, the metal does not significantly expand till melting. Despite the fact that, on the whole, the dynamical stability of Cu, Au, and Pt lattices at $\rho = \rho_0$ increases as T_e elevates, the accuracy of current experiments does not allow the detection of their lattice hardening.

[1] C. W. Siders, A. Cavalleri, K. Sokolowski-Tinten, C. Tóth, T. Guo, M. Kammler, M. H. von Hoegen, K. R. Wilson, D. von der Linde, and C. P. J. Barty, Science **286**, 1340 (1999).

[2] B. J. Siwick, J. R. Dwyer, R. E. Jordan, and R. J. D. Miller, Science **302**, 1382 (2003).

[3] M. Harb, R. Ernstorfer, C. T. Hebeisen, G. Sciaini, W. Peng, T. Dartigalongue, M. A. Eriksson, M. G. Lagally, S. G. Kruglik, and R. J. Dwayne Miller, Phys. Rev. Lett. **100**, 155504 (2008).

[4] R. Ernstorfer, M. Harb, C. T. Hebeisen, G. Sciaini, T. Dartigalongue, and R. J. D. Miller, Science **323**, 1033 (2009).

[5] G. Sciaini, M. Harb, S. G. Kruglik, T. Payer, C. T. Hebeisen, F.-J. M. zu Heringdorf, M. Yamaguchi, M. H. von Hoegen, R. Ernstorfer, and R. J. D. Miller, Nature (London) **458**, 56 (2009).

[6] R. J. D. Miller, Science **343**, 1108 (2014).

[7] M. Z. Mo, Z. Chen, R. K. Li, M. Dunning, B. B. L. Witte, J. K. Baldwin, L. B. Fletcher, J. B. Kim, A. Ng, R. Redmer, A. H. Reid, P. Shekhar, X. Z. Shen, M. Shen, K. Sokolowski-Tinten, Y. Y. Tsui, Y. Q. Wang, Q. Zheng, X. J. Wang, and S. H. Glenzer, Science **360**, 1451 (2018).

[8] J. Hohlfeld, S.-S. Wellershoff, J. Güdde, U. Conrad, V. Jähnke, and E. Matthias, Chem. Phys. **251**, 237 (2000).

[9] Z. Chen, V. Sametoglu, Y. Y. Tsui, T. Ao, and A. Ng, Phys. Rev. Lett. **108**, 165001 (2012).

[10] V. Recoules, J. Clérouin, G. Zérah, P. M. Anglade, and S. Mazevet, Phys. Rev. Lett. **96**, 055503 (2006).

[11] F. Cheenicode Kabeer, E. S. Zijlstra, and M. E. Garcia, Phys. Rev. B **89**, 100301(R) (2014).

[12] D. V. Minakov and P. R. Levashov, Phys. Rev. B **92**, 224102 (2015).

[13] S. L. Daraszewicz, Y. Giret, N. Naruse, Y. Murooka, J. Yang, D. M. Duffy, A. L. Shluger, and K. Tanimura, Phys. Rev. B **88**, 184101 (2013).

[14] S. I. Anisimov, B. L. Kapeliovich, and T. L. Perel'man, Zh. Eksp. Teor. Fiz. **66**, 776 (1974) [Sov. Phys. JETP **39**, 375 (1974)].

[15] D. S. Ivanov and L. V. Zhigilei, Phys. Rev. B **68**, 064114 (2003).

[16] G. E. Norman, S. V. Starikov, and V. V. Stegailov, J. Exp. Theor. Phys. **114**, 792 (2012).

[17] M. E. Povarnitsyn, V. B. Fokin, P. R. Levashov, and T. E. Itina, Phys. Rev. B **92**, 174104 (2015).

[18] X. Y. Wang, D. M. Riffe, Y.-S. Lee, and M. C. Downer, Phys. Rev. B **50**, 8016 (1994).

[19] Z. Lin, L. V. Zhigilei, and V. Celli, Phys. Rev. B **77**, 075133 (2008).

[20] L. Waldecker, R. Bertoni, R. Ernstorfer, and J. Vorberger, Phys. Rev. X **6**, 021003 (2016).

[21] B. I. Cho, T. Ogitsu, K. Engelhorn, A. A. Correa, Y. Ping, J. W. Lee, L. J. Bae, D. Prendergast, R. W. Falcone, and P. A. Heimann, Sci. Rep. **6**, 18843 (2016).

[22] W. L. McMillan, Phys. Rev. **167**, 331 (1968).

[23] P. B. Allen, Phys. Rev. Lett. **59**, 1460 (1987).

[24] I. Y. Sklyadneva, R. Heid, P. M. Echenique, K.-B. Bohnen, and E. V. Chulkov, Phys. Rev. B **85**, 155115 (2012).

[25] S. Y. Savrasov and D. Y. Savrasov, Phys. Rev. B **54**, 16487 (1996).

[26] S. Poncé, E. R. Margine, C. Verdi, and F. Giustino, Comp. Phys. Commun. **209**, 116 (2016).

[27] M. I. Kaganov, I. M. Lifshitz, and L. V. Tanatarov, Zh. Eksp. Teor. Fiz. **31**, 232 (1956) [Sov. Phys. JETP **4**, 173 (1957)].

[28] S. Y. Savrasov, Phys. Rev. B **54**, 16470 (1996).

[29] N. A. Smirnov, J. Phys.: Condens. Matter **29**, 105402 (2017).

[30] R. Briggs, F. Coppari, M. G. Gorman, R. F. Smith, S. J. Tracy, A. L. Coleman, A. Fernandez-Panella, M. Millot, J. H. Eggert, and D. E. Fratanduono, Phys. Rev. Lett. **123**, 045701 (2019).

[31] J. Sólyom, *Fundamentals of the Physics of Solids* (Springer, Berlin, 2009), Vol. 1.

[32] S. Mazevet, J. Clérouin, V. Recoules, P. M. Anglade, and G. Zerah, Phys. Rev. Lett. **95**, 085002 (2005).

[33] K.-H. Hellwege and O. Madelung (Eds.), *Phonon States of Elements. Electron States and Fermi Surfaces of Alloys*, Landolt-Börnstein, New Series, Group III, Vol. 13 Pt. a (Springer, Berlin, 1981).

[34] O. Gunnarsson and B. Lundqvist, Phys. Rev. B **13**, 4274 (1976).

[35] J. P. Perdew, J. A. Chevary, S. H. Vosko, K. A. Jackson, M. R. Pederson, D. J. Singh, and C. Fiolhais, Phys. Rev. B **46**, 6671 (1992); **48**, 4978(E) (1993).
[36] J. P. Perdew, *Electronic Structure of Solids '91* (Akademie, Berlin, 1991), p. 11.
[37] J. P. Perdew, A. Ruzsinszky, G. I. Csonka, O. A. Vydrov, G. E. Scuseria, L. A. Constantin, X. Zhou, and K. Burke, Phys. Rev. Lett. **100**, 136406 (2008).
[38] P. A. Loboda, N. A. Smirnov, A. A. Shadrin, and N. G. Karlykhanov, High Energy Density Phys. **7**, 361 (2011).
[39] P. E. Blöchl, O. Jepsen, and O. K. Andersen, Phys. Rev. B **49**, 16223 (1994).
[40] K. P. Migdal, Y. V. Petrov, and N. A. Inogamov, Proc. SPIE **9065**, 906503 (2013).
[41] J. Simoni and J. Daligault, Phys. Rev. Lett. **122**, 205001 (2019).
[42] M. Z. Mo, V. Becker, B. K. Ofori-Okai, X. Shen, Z. Chen, B. Witte, R. Redmer, R. K. Li, M. Dunning, S. P. Weathersby, X. J. Wang, and S. H. Glenzer, Rev. Sci. Instrum. **89**, 10C108 (2018).
[43] H. E. Elsayed-Ali, T. B. Norris, M. A. Pessot, and G. A. Mourou, Phys. Rev. Lett. **58**, 1212 (1987).
[44] S. D. Brorson, A. Kazeroonian, J. S. Moodera, D. W. Face, T. K. Cheng, E. P. Ippen, M. S. Dresselhaus, and G. Dresselhaus, Phys. Rev. Lett. **64**, 2172 (1990).
[45] Y. V. Petrov, N. A. Inogamov, and K. P. Migdal, JETP Lett. **97**, 20 (2013).
[46] Y. Shen, T. Gao, and M. Wang, Comp. Mater. Sci. **77**, 372 (2013).
[47] W. M. Heynes (Ed.), *CRC Handbook of Chemistry and Physics* (CRC, Boca Raton, FL, 2010).
[48] C.-M. Liu, X.-R. Chen, C. Xu, L.-C. Cai, and F.-Q. Jing, J. Appl. Phys. **112**, 013518 (2012).
[49] E. Bévillon, J. Colombier, V. Recoules, and R. Stoian, Appl. Surf. Sci. **336**, 79 (2015).
[50] G. V. Sin'ko, N. A. Smirnov, A. A. Ovechkin, P. R. Levashov, and K. V. Khishchenko, High Energy Density Phys. **9**, 309 (2013).
[51] Z. Lin and L. V. Zhigilei, Phys. Rev. B **73**, 184113 (2006).
[52] M. G. Pamato, I. G. Wood, D. P. Dobson, S. A. Hunt, and L. Vočadlo, J. Appl. Crystallogr. **51**, 470 (2018).
[53] J. R. Dwyer, C. T. Hebeisen, R. Ernstorfer, M. Harb, V. B. Deyirmenjian, R. E. Jordan, and R. J. D. Miller, Philos. Trans. R. Soc. London Sect. A **364**, 741 (2006).
[54] M. Mo, S. Murphy, Z. Chen, P. Fossati, R. Li, Y. Wang, X. Wang, and S. Glenzer, Sci. Adv. **5**, eaaw0392 (2019).
[55] A. P. Caffrey, P. E. Hopkins, J. M. Klopf, and P. M. Norris, Micro. Thermophys. Eng. **9**, 365 (2005).
[56] A. B. Belonoshko and A. Rosengren, Phys. Rev. B **85**, 174104 (2012).
[57] S. Anzellini, V. Monteseguro, E. Bandiello, A. Dewaele, L. Burakovsky, and D. Errandonea, Sci. Rep. **9**, 13034 (2019).
[58] D. Errandonea, Phys. Rev. B **87**, 054108 (2013).
[59] K. A. Gschneidner, *Solid State Physics* (Academic, New York, 1964), Vol. 16, p. 275.